

Can an Actor-Critic Optimization Framework Improve Analog Design Optimization?

Sounak Dutta*, Fin Amin*, Sushil Panda, Jonathan Rabe, Yuejiang Wen, Paul Franzon
Department of Electrical and Computer Engineering
North Carolina State University
{sdutta6, samin2, spanda4, jcrabe, wyuejia, paulf}@ncsu.edu

Abstract—Analog design often slows down because even small changes to device sizes or biases require expensive simulation cycles, and high-quality solutions typically occupy only a narrow part of a very large search space. While existing optimizers reduce some of this burden, they largely operate without the kind of judgment designers use when deciding where to search next. This paper presents an actor-critic optimization framework (ACOF) for analog sizing that brings that form of guidance into the loop. Rather than treating optimization as a purely black-box search problem, ACOF separates the roles of proposal and evaluation: an actor suggests promising regions of the design space, while a critic reviews those choices, enforces design legality, and redirects the search when progress is hampered. This structure preserves compatibility with standard simulator-based flows while making the search process more deliberate, stable, and interpretable. Across our test circuits, ACOF improves the top-10 figure of merit by an average of 38.9% over the strongest competing baseline and reduces regret by an average of 24.7%, with peak gains of 70.5% in FoM and 42.2% lower regret on individual circuits. By combining iterative reasoning with simulation-driven search, the framework offers a more transparent path toward automated analog sizing across challenging design spaces.

Index Terms—analog circuit optimization, Bayesian optimization, Large language models, SPICE simulation

I. INTRODUCTION AND MOTIVATION

The demands on modern analog design continue to increase with new technology nodes, tighter specifications, and faster development cycles. Each node changes transistor behavior, invalidates earlier biasing strategies, and requires renewed exploration of the design space. From an optimization standpoint, this is no longer merely schematic tuning, but the search for a feasible region where gain, bandwidth, phase margin, and power can be satisfied together. Because performance varies nonlinearly with sizing, designers need SPICE simulations, and more knobs mean more costly trials. Even after the topology is fixed, analog sizing is rarely straightforward. It typically requires repeated evaluation and careful adjustment to satisfy several coupled specifications while managing trade-offs among performance, power, and area. In practice, analog design is still a slow and labor-intensive process, requiring extensive simulation and considerable designer expertise [1]–[3].

* Equal contribution.

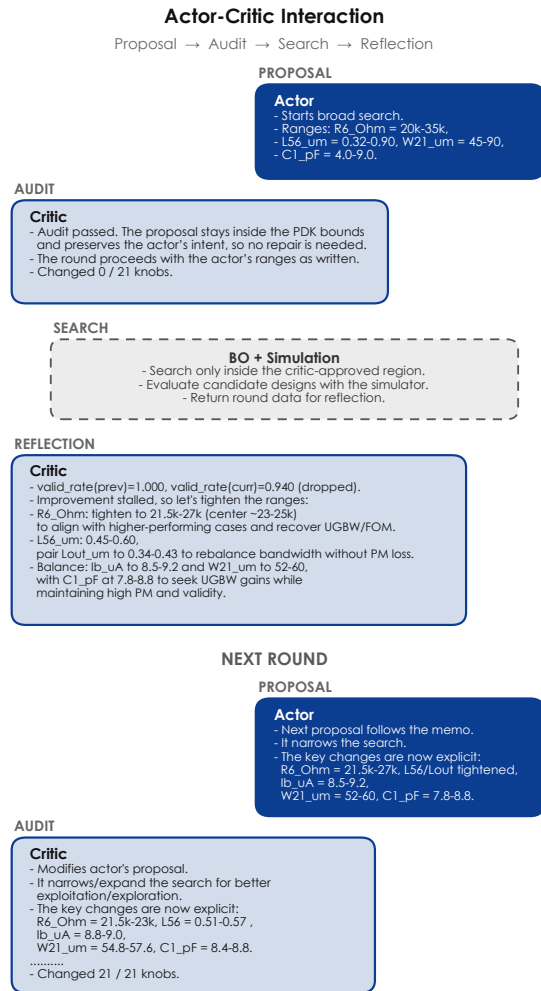


Fig. 1. Example of interactions between our actor and critic components over rounds during analog sizing optimization. Our framework defines a closed-loop optimization process that alternates between proposal, audit, search, and reflection.

For that reason, analog sizing has long been viewed as a constrained optimization problem. From that perspective, the central challenge is not simply to evaluate better candidate points, but to direct the search toward regions of the design space that are more likely to produce feasible and high-performing solutions under competing design constraints [2]–

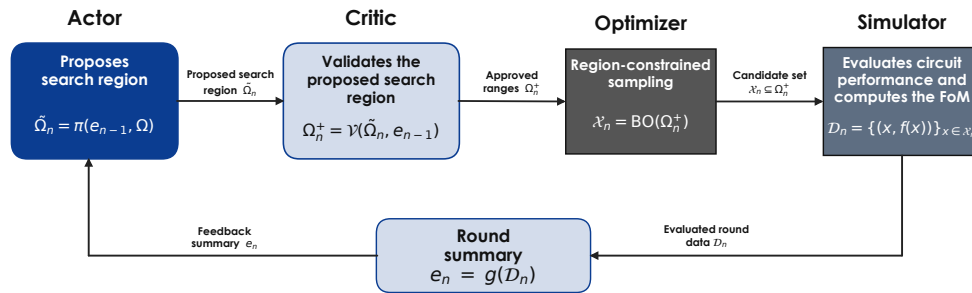


Fig. 2. An overview of our actor–critic optimization framework (ACOF). At each time step, n , the actor proposes a candidate search region $\tilde{\Omega}_n$, the critic adjusts it to a PDK-legal region Ω_n^+ , BO selects candidates $x \in \Omega_n^+$ for simulation, and simulator outcomes are summarized into e_n for the next round. ACOF is agnostic to the specific choice of BO.

[5]. Human designers address this problem differently. They do not treat the search space as uniformly promising; they use judgment to focus attention, interpret trade-offs, and revise direction when progress stalls.

This paper is motivated by the idea that such guidance should become part of the optimization loop itself. Recent LLM-based studies in electronic design suggest that language models can contribute to design automation as reasoning agents rather than as mere text generators [6]–[11]. Building on that perspective, **our contribution** is investigating casting analog sizing as an actor–critic process in which one agent proposes promising regions of the design space, another evaluates whether the search direction should be preserved or revised, and a conventional optimizer explores within the resulting region. In this way, automated analog sizing can become not only more sample-efficient, but also more interpretable and more aligned with the way experienced designers reason about difficult trade-offs.

II. PRIOR ART

A. Bayesian Optimization for Analog Circuit Sizing

Bayesian optimization (BO) has advanced analog circuit sizing in several important ways [12]. WEIBO [4] formulates sizing as constrained BO with Gaussian-process (GP) surrogates and weighted expected improvement, and extends the approach to multi-objective design. Local BO [5] scales this idea to larger spaces through trust-region-based local models and batch candidate evaluation. tSS-BO [13] targets the high-dimensional setting by restricting search to an effective truncated subspace while retaining local GP guidance and Bayesian selection.

B. Language Driven Optimization

Recent LLM-based work in analog design has begun to open several distinct directions rather than one unified path. LayoutCopilot [6] reimagines analog layout interaction by turning natural-language design requests into executable layout actions through a multi-agent framework, while LLANA [7] brings language models into the BO loop to generate design-dependent layout constraints, particularly net-weighting parameters for layout synthesis. AmpAgent [8] approaches amplifier design as a coordinated reasoning process across

literature understanding, formula derivation, and device sizing. In contrast, AnalogCoder [9] treats analog design as a code-generation problem, using a training-free workflow to produce and iteratively correct Python-based circuit implementations. ADO-LLM [10] more directly couples an LLM with Bayesian optimization for circuit sizing, using the model to propose promising design candidates alongside a GP-based search process. LEDRO [14], in turn, shifts the emphasis from asking the LLM for a single sizing answer to asking it to progressively narrow the search region so that optimization can proceed within a more meaningful part of the design space. More recent frameworks extend this picture in complementary ways: EEsizer [15] formulates transistor sizing as a closed-loop LLM-guided process built around simulation, analysis, and iterative parameter updates, while LLM-USO [16] focuses on structured knowledge reuse across related circuits.

C. Takeways from Prior Art

These prior works point to the same recurring pressures: GP-based BO becomes harder to scale as the sample set and parameter dimension grow. Constrained search remains difficult, and exploration becomes increasingly fragile in high-dimensional spaces. Furthermore, these methods mainly act as black boxes [5], [7], [13]. Recent LLM-based methods have begun to address these limitations in different ways: some strengthen the reasoning and decomposition side of analog design [8], some couple LLMs with BO to improve candidate generation within the optimization loop [10] and some demonstrate the broader value of self-reflection [17] for iterative improvement in workflows using optimizer [14]. But in these systems, guidance is still driven mainly by simulator feedback or by the model’s own reflective process, leaving a natural opening for an independent critic that can examine a proposal from outside the actor’s reasoning stream. That distinction matters because prompt-heavy LLM systems already report performance dilution under long, multitask context [6]. In relation to this, long-context retrieval studies show that current LLMs can struggle even on simple fact-retrieval tasks as context grows [18]. Our method is designed around exactly this gap. Considering these takeaways, we introduce ACOF in the following section.

TABLE I

RESULTS ACROSS THE FOUR TEST CIRCUITS, AGGREGATED OVER 3 RUNS PER CIRCUIT. EACH CIRCUIT FORMS ONE MULTIROW BLOCK AT LEFT. VALUES ARE MEAN WITH SUBSCRIPTED SEM (STANDARD ERROR OF THE MEAN). BOLD INDICATES THE BEST BASELINE METHOD WITHIN EACH CIRCUIT AND METRIC. QWEN WAS USED AS THE LLM.

Method	Top-10 Design Quality					Reliability (%)		Exploration/Exploitation		
	Gain (dB) \uparrow	UGBW (MHz) \uparrow	PM (deg) \uparrow	Power (mW) \downarrow	FoM \uparrow	Sim. Valid \uparrow	Phys. Feasible \uparrow	Regions \uparrow	Regret \downarrow	
130nm 12 Params	Target Spec.	85.00	900.00	100.00	0.554	0.00	-	-	-	-
	ACOF	83.65 _{0.64}	785.30 _{39.71}	101.35 _{1.13}	0.658 _{0.045}	-0.19 _{0.01}	97.0 _{0.1}	86.2 _{1.4}	2.0 _{0.0}	0.25 _{0.01}
	Single-LLM	83.15 _{0.55}	717.63 _{45.51}	111.89 _{0.74}	0.657 _{0.029}	-0.24 _{0.02}	95.4 _{0.9}	78.9 _{1.8}	2.7 _{0.3}	0.30 _{0.01}
	Pure-BO	76.24 _{1.45}	673.92 _{22.65}	128.23 _{3.27}	0.587 _{0.014}	-0.39 _{0.02}	81.0 _{0.3}	26.9 _{0.1}	3.0 _{0.8}	0.37 _{0.02}
	Human Expert	72.77	851.48	173.59	0.821	-0.45	-	-	-	-
180nm 12 Params	Target Spec.	95.00	500.00	100.00	0.194	0.00	-	-	-	-
	ACOF	90.99 _{0.55}	195.59 _{10.25}	119.77 _{2.23}	0.200 _{0.001}	-0.52 _{0.02}	100.0 _{0.0}	90.2 _{1.9}	5.0 _{1.2}	0.59 _{0.02}
	Single-LLM	90.88 _{0.20}	240.69 _{78.42}	117.72 _{1.86}	0.324 _{0.104}	-0.64 _{0.01}	100.0 _{0.0}	84.9 _{1.0}	2.0 _{0.0}	0.64 _{0.01}
	Pure-BO	86.79 _{0.29}	253.71 _{7.97}	127.97 _{1.23}	0.359 _{0.024}	-0.74 _{0.02}	96.1 _{0.5}	36.1 _{2.6}	2.0 _{0.0}	0.69 _{0.04}
	Human Expert	81.62	365.69	127.42	0.361	-0.68	-	-	-	-
130nm 17 Params	Target Spec.	85.00	20.00	100.00	0.277	0.00	-	-	-	-
	ACOF	88.56 _{2.77}	29.45 _{7.68}	104.59 _{22.57}	0.290 _{0.008}	-0.13 _{0.05}	97.7 _{0.8}	81.7 _{10.3}	3.7 _{0.7}	0.26 _{0.02}
	Single-LLM	87.06 _{1.53}	20.62 _{1.04}	71.73 _{2.23}	0.475 _{0.141}	-0.44 _{0.17}	93.9 _{1.6}	82.3 _{6.5}	2.7 _{0.5}	0.45 _{0.12}
	Pure-BO	85.69 _{0.40}	50.49 _{15.61}	74.93 _{5.47}	0.656 _{0.100}	-0.73 _{0.01}	84.6 _{0.6}	68.4 _{0.6}	1.3 _{0.5}	0.65 _{0.03}
	Human Expert	78.33	9.93	80.06	0.560	-0.91	-	-	-	-
180nm 21 Params	Target Spec.	85.00	1200.00	120.00	1.320	0.00	-	-	-	-
	ACOF	94.57 _{2.38}	1095.36 _{18.60}	84.20 _{3.69}	1.329 _{0.014}	-0.24 _{0.02}	99.3 _{0.3}	85.6 _{2.4}	2.7 _{0.3}	0.32 _{0.01}
	Single-LLM	102.43 _{4.70}	759.88 _{178.60}	90.91 _{10.95}	1.232 _{0.090}	-0.44 _{0.07}	99.7 _{0.2}	74.6 _{3.3}	1.0 _{0.8}	0.47 _{0.05}
	Pure-BO	98.06 _{2.13}	469.33 _{59.13}	123.24 _{7.15}	1.243 _{0.068}	-0.61 _{0.01}	91.4 _{0.1}	19.3 _{1.0}	1.7 _{0.7}	0.58 _{0.01}
	Human Expert	72.69	1138.87	124.78	2.210	-0.51	-	-	-	-

III. OUR APPROACH

We formulate analog circuit design optimization as $x^* = \arg \max_{x \in \Omega} f(x)$, where x denotes the vector of tunable circuit parameters, Ω denotes the global feasible design domain induced by technology bounds and hard circuit constraints, which is primarily defined by the PDK and $f(x)$ denotes the scalar figure of merit (FoM) obtained from circuit simulation.

Our approach, the actor-critic optimization framework (ACOF), is organized as a role-separated reasoning loop with two logical agents: an *actor*, which proposes where the search should move next, and a *critic*, which reviews that proposal before optimization proceeds. This structure turns the familiar design-review pattern of analog practice into an iterative computational procedure.

In our pipeline the actor does not output a single design point; instead, it proposes a search region within which the downstream optimizer should explore. At initialization, the actor is seeded by a small set of valid calibration examples, denoted by \mathcal{C}_0 [14], and produces the first candidate region $\tilde{\Omega}_1 = \pi(\mathcal{C}_0, \Omega)$. After the first round, the actor is updated by a round summary e_{n-1} that condenses what the previous round revealed, including the best design found so far, representative high-quality samples, and the critic’s reflection on that round, so that for later rounds it proposes $\tilde{\Omega}_n = \pi(e_{n-1}, \Omega)$. In the implemented loop, the actor is therefore driven not by the previous corrected region itself, but by the evidence generated

from searching within it. Instead of allowing optimization to unfold as a blind sequence of samples, ACOF inserts an explicit stage of judgment between proposal and evaluation. As the search progresses, the critic also produces short reflection memos [17] that capture recurring patterns, useful corrections, and promising directions, thereby giving the loop continuity across rounds. An overview is given in Fig. 2.

Before any BO step is performed, the critic audits the actor’s proposal and converts it into the region actually used for search, written as $\Omega_n^+ = \mathcal{V}(\tilde{\Omega}_n, e_{n-1})$, where $\mathcal{V}(\cdot)$ denotes the critic’s validation and correction step. Here Ω_n^+ is the post-audit region for round n : it is the actor’s proposal after being checked, corrected when necessary, and accepted for optimization. Conceptually, this stage both preserves the actor’s intent when that intent is coherent and stabilizes the search when the proposal is malformed, overly narrow, overly loose, or otherwise inconsistent with the feasible domain. In this sense, the critic functions less as a second optimizer than as a gatekeeper that keeps exploration disciplined.

Once Ω_n^+ has been established, BO and simulation are carried out within that region under a fixed evaluation budget. $\mathcal{X}_n \sim \text{BO}(\Omega_n^+)$ denotes the candidate designs selected for evaluation in round n , then simulation produces the round data set $\mathcal{D}_n = \{(x, f(x))\}_{x \in \mathcal{X}_n}$, where $f(x)$ is the desired figure of merit. BO is therefore not used to search the full design space at every step, but to search efficiently within the region approved

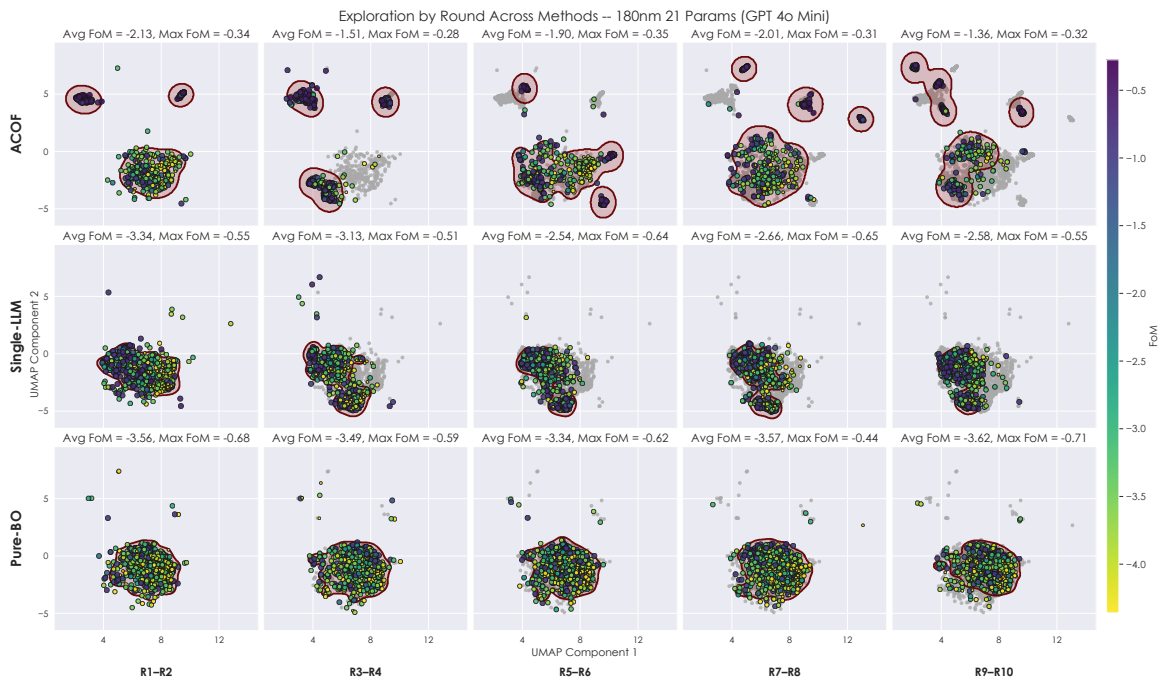


Fig. 3. UMAP projections of the sizing parameters illustrate how the design space was explored over optimization rounds. To aid visualization, we outlined regions being explored in the current rounds in red and rendered the cumulative explored designs from past rounds in gray. ACOF judiciously explores the design space by targeting regions corresponding to high performance—as indicated by the higher round-wise Avg and Max FoM. Our technique successfully explored the regions above UMAP Component 2 > 1. On the other hand, the Single-LLM and Pure-BO baselines were apprehensive to exploration and achieved worse FoMs.

for that round.

After simulation, the framework compresses the round’s outcomes into a summary $e_n = g(\mathcal{D}_n)$, where $g(\cdot)$ denotes the round-level reflection process. This summary captures the practical meaning of the round: which parts of the region were productive, whether progress was made, and what kind of adjustment should guide the next proposal. The critic’s memo is part of this summary, so the feedback is not purely numerical but also interpretive. The next round then follows the same pattern, with $\Omega_{n+1} = \pi(e_n, \Omega)$ and $\Omega_{n+1}^+ = \mathcal{V}(\Omega_{n+1}, e_n)$.

Taken together, these steps define a closed-loop optimization process that alternates between proposal, audit, search, and reflection (see Fig. 1). The actor proposes where to search, the critic determines whether that proposal is suitable for actual optimization, BO explores within the approved region, and the resulting evidence is distilled into guidance for the next round. This separation between proposing a region and approving a region is the core operational idea of ACOF: it allows the search space to be refined progressively while remaining anchored to the feasible structure of the circuit.

A. Why Use an Actor-Critic Structure?

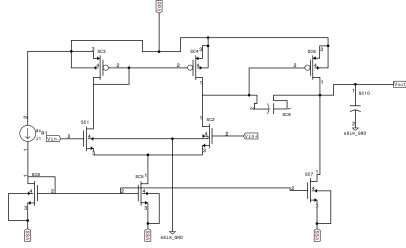
The distinction between policy-based and value-based methods provides a useful lens for understanding why an actor-critic structure is a natural design choice in optimization. In reinforcement learning (RL), policy methods learn a direct mapping from states to actions, whereas value-based methods learn an estimate of expected return to guide action selection, as in REINFORCE/TRPO versus Q-learning/DQN [19]–[22]. The

historical trend was not a simple shift from policy learning to value learning, since value-based deep RL was already central in the mid-2010s through DQN. A more meaningful shift was toward methods in which action proposals are shaped by an explicit evaluator. Actor-critic methods made this especially clear by pairing a policy with a learned critic that scores actions or states and stabilizes learning through lower-variance updates [20], [23]. More broadly, this points to a lesson larger than any one RL algorithm: many successful learning systems benefit when generation and judgment need not share the same mechanism. Methods such as Soft Actor-Critic, TD3, and MuZero push this logic further by placing learned value estimates, critics, and planning modules at the center of decision making [23]–[25]. In parallel, reward-learning and preference-based frameworks, including RLHF, further reinforce the idea that learning what should evaluate behavior can be as important as learning the behavior itself [26], [27].

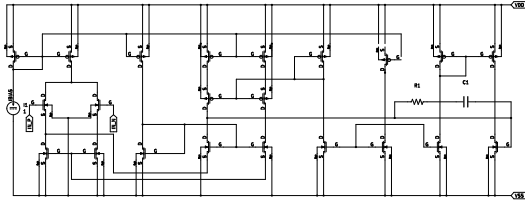
Our approach is motivated by the same principle, but applied to analog sizing rather than sequential control. Our framework is not an RL algorithm in the standard sense; instead, it adopts the structural lesson behind actor-critic methods by separating the proposal of a search region from its evaluation. In analog optimization, this separation is useful because a proposed region may be promising in spirit yet still be ill-posed, physically implausible, or wasteful under a fixed simulation budget. An independent critic therefore serves as an explicit evaluative mechanism that helps stabilize and redirect the search before expensive simulation is spent.

IV. EXPERIMENTS

We evaluate three optimization frameworks for their effectiveness in identifying high-quality circuit designs. In all cases, the objective is to maximize a scalar FoM that captures the target performance requirements. For each circuit, run, and method, we form a run-level summary, and then we report the average and standard error of the run-level summaries across the three runs. Our analysis considers three groups of metrics: design quality, reliability, and exploration/exploitation.



(a) Two-stage amplifier



(b) Folded cascode single-ended amplifier

Fig. 4. The circuit schematics of our benchmarks. For an OpAmp, gain, bandwidth, phase margin, and power are coupled design specifications. Higher DC gain can introduce additional poles; this affects phase margin. Also, improving UGBW usually requires a higher bias current and increases power. Since low power is desirable, the circuit must balance gain, UGBW, and power, while phase margin sets the stability constraint and often trades off with frequency response and bandwidth.

A. Benchmarks

We benchmark four circuits of varying complexity across two technology nodes. In SKY130 (130 nm), we consider a two-stage amplifier and a cascode wide-swing amplifier with design vectors $x \in \mathbb{R}^{12}$ and $x \in \mathbb{R}^{17}$, respectively. In GF180MCU (180 nm), we consider a two-stage amplifier and a folded-cascode single-ended amplifier with design vectors $x \in \mathbb{R}^{12}$ and $x \in \mathbb{R}^{21}$, respectively (see Fig. 4). Each design vector includes the tunable devices, bias, and compensation parameters.

B. Implementations and Baselines

The first setup employs the proposed ACOF. For comparison, we use a second setup that replaces the actor–critic loop with a single LLM coupled to the same BO backend, and a third setup that uses BO alone with no LLM guidance. All three methods follow the same round schedule and the same per-round simulation budget under identical circuit-simulation conditions. In **ACOF**, the actor and critic are prompted separately. The actor is given topology-specific context, and the calibration set from the first round or a packed summary of the strongest

valid designs from the previous round, including gain, UGBW, phase margin, power, and operating-region information. It then proposes numeric subranges for all tunable parameters. The critic receives those proposed ranges and returns a structured audit that either accepts the actor ranges or repairs them minimally within the legal bounds before BO is launched. After BO evaluates the candidate designs in the critic-approved region, the round summary is written back into the next actor prompt so that the search region can be revised progressively rather than reinitialized from scratch. See Fig. 1 for an example. **For clarity and reproducibility, we will release the full prompting templates upon acceptance.**

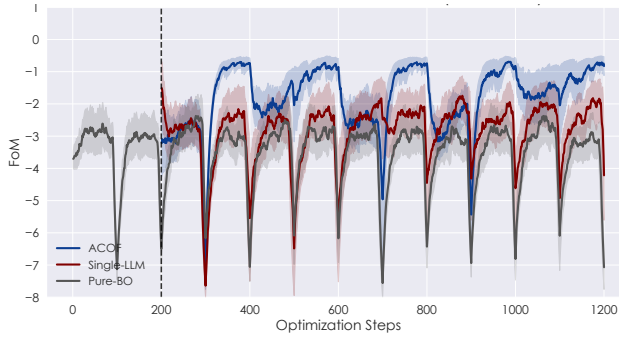
Inspired by LEDRO [14], we implement a **Single-LLM** baseline to interface with BO. At each step it performs the actor’s candidate search region step but forgoes the correction/refinement by the critic. Lastly, as an LLM-free comparison, we report the performance of **Pure-BO**, by optimizing the design using BO, [28]. Before the rounds begin, an initial set of designs is generated using BO to provide $C_0 = 200$ starting points, which are used to condition the LLM baselines. In each round, we perform the optimization procedures and use Ngspice to compute the FoMs [29]. In our experiments, we configure our LLM-based methods using the open-source Qwen2.5-14B-Instruct [30]. To see how performance changes with respect to stronger LLM capabilities, we rerun our experiments on the 21-parameter folded-cascode benchmark using GPT-4o-mini [31] and GPT-5 [32].

C. Performance Metrics

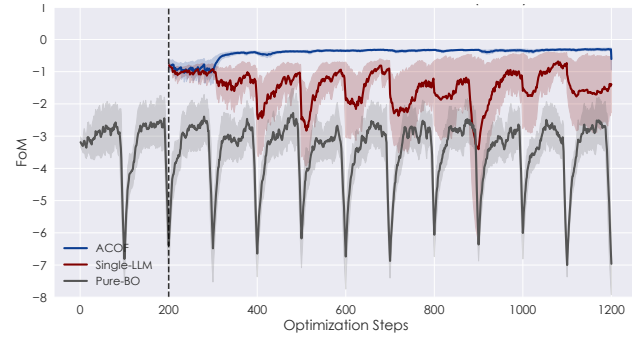
Design Quality. We measure and maximize FoM computed from gain $G(x)$, unity-gain bandwidth $BW(x)$, phase margin $\phi(x)$, and power $W(x)$. We define circuit-specific targets (G^*, BW^*, ϕ^*, W^*) , reported as Target Spec. in Fig. 1, and use them to construct normalized component scores $s_G(x)$, $s_{BW}(x)$, $s_\phi(x)$, and $s_W(x)$. Each score is zero when its corresponding target is met and penalizes deviations otherwise; we then combine them as $f(x) = 3 \cdot s_G(x) + s_{BW}(x) + s_\phi(x) + s_W(x)$. These quantities are not reported from a single best design. Instead, for each run and method, we sort all simulated designs by FoM and average each metric over the top-10 designs in our experiments. This gives a more stable summary of the quality of the best part of the search than reporting only a single extreme point.

Reliability. We report two run-level rates. *Sim. Valid* is the fraction of all attempted designs in a run whose simulator output was marked valid by the pipeline. *Phys. Feasible* is the fraction of attempted designs that satisfy our physical sanity checks. In our implementation, a design is counted as physically meaningful only if it yields positive bandwidth, positive phase margin, positive power, and nonnegative gain. Both reliability metrics are computed over the full set of attempts.

Exploration/Exploitation. To summarize how broadly each method visits distinct parts of the design space, we report *Regions*. For each circuit, we first normalize the active design parameters to $[0, 1]$ using that circuit’s own parameter ranges. We then pool all sampled designs from a given run and method,



(a) GPT 4o Mini. Average and SEM of Top-10 FoM: **ACOF** -0.359 ± 0.018 , **Single-LLM** -0.643 ± 0.015 , **Pure-BO** -0.652 ± 0.026 .



(b) GPT 5. Average and SEM of Top-10 FoM: **ACOF** -0.271 ± 0.024 , **Single-LLM** -0.319 ± 0.035 , **Pure-BO** -0.639 ± 0.019 .

Fig. 5. Exponentially-smoothed FoM trajectories for the 180nm 21-parameter folded-cascade benchmark using variants of GPT as the LLM. Subcaptions report the across-run mean of the per-run top-10 mean FOM. Optimization steps for the LLM-based methods begin at 200 because both are initialized with $C_0 = 200$ seed designs generated by Pure-BO. After initialization, the LLM-based methods update the optimization ranges every 100 steps.

TABLE II
RESULTS ON THE 180NM 21-PARAMETER FOLDED-CASCADE BENCHMARK USING VARIANTS OF GPT AS THE LLM.

Model	Method	Top-10 FoM \uparrow	Phys. Feasible (%) \uparrow	Regret \downarrow
GPT-4o Mini	ACOF	-0.359 _{0.018}	67.1 _{3.5}	0.395 _{0.019}
	Single-LLM	-0.643 _{0.015}	37.8 _{2.3}	0.579 _{0.021}
GPT-5	ACOF	-0.271 _{0.024}	99.4 _{0.0}	0.313 _{0.019}
	Single-LLM	-0.319 _{0.035}	80.9 _{8.9}	0.381 _{0.024}

and apply HDBSCAN [33], an unsupervised clustering method, in the normalized design space. The reported value is the number of discovered regions. A larger value indicates that the method visited more distinct regions of the parameter space during the run. This metric is computed from the full run-level point cloud. We also report *Regret*, defined relative to the ideal FoM value of 0. For each run and method, at each step we compute the gap between 0 and the best FoM found up to that point, and report the average of that quantity over the run. Lower regret means that the method reached strong designs earlier and stayed closer to the ideal score throughout the run.

V. DISCUSSION AND CONCLUSION

Across all four benchmarks in Table I, ACOF is the only method that remains on top in both FoM and regret. That pattern is more revealing than any one raw specification because the table reports averages over the top-10 designs, so the indication comes from the quality of a region rather than from a single fortunate sample. The baselines do lead on isolated metrics from time to time—Pure-BO on phase margin in some cases and on bandwidth in two circuits, and Single-LLM on gain for the 180 nm 21-parameters benchmark—but those wins do not carry through to the joint objective. ACOF repeatedly converges to design sets in which gain, bandwidth, stability, and power sit in a better overall balance.

Fig. 5 shows a similar overall trend. After the shared initialization budget, ACOF rises to stronger FoM levels and remains there through most of the search. In Fig. 5a, ACOF is

44.2% closer to the ideal FoM of 0 than Single-LLM and 44.9% closer to 0 than Pure-BO. In Fig. 5b, the LM-guided portion shifts upward further: ACOF improves again, Single-LLM also benefits from the stronger model, and Pure-BO remains nearly unchanged. This result shows that the framework is not tied to one particular LM and that a better underlying model can be converted into better optimization behavior without changing the search procedure.

The reliability columns in Table I tell a similar story. ACOF stays at or near perfect simulator validity throughout the study, but the more informative quantity is physical feasibility. On the 180 nm 21-parameters circuit, nearly every ACOF proposal simulates, and a much larger fraction remains physically meaningful than for Single-LLM or Pure-BO. The same trend is visible on the 130 nm 12-parameters and 180 nm 12-parameters benchmarks as well. Viewed alongside the actor-critic exchange in Fig. 1, this suggests that the critic is affecting what gets tried next, not merely repairing malformed outputs. In practice, that means fewer simulations are spent on points that are admissible yet unhelpful from an analog-design standpoint.

The same search trend is visible in both the Table I and Fig. 3. On the 180 nm 21-parameters circuit, the red contours for ACOF migrate across several separated pockets of the embedding over successive round pairs, including pockets at UMAP Component 2 > 1 in Fig. 3—a region that the baselines touch lightly. What matters is that these relocations remain productive. In every round pair, the ACOF panels report a better average FoM than the corresponding Single-LLM and Pure-BO panels, and the best FoM found within each pair is stronger as well. Table I quantifies this behavior using Qwen as the LLM. On this benchmark ACOF covers the largest number of regions and still records the best FoM and regret. A similar relation between region coverage and solution quality appears on the 180 nm 12-parameters and 130 nm 17-parameters circuits, where ACOF also visits more regions than either baseline. The 130 nm 12-parameters case is instructive in the opposite direction: Pure-BO touches the most regions there, yet its physical-feasibility rate falls to 26.9%. The useful

distinction is therefore not movement alone, but movement that lands in workable territory. ACOF shifts when a new region is needed and stays with a region when it is still yielding good designs.

Taken together, Table I, Fig. 3, and Fig. 5 support the same conclusion. ACOF spends more of the evaluation budget in parts of the design space that are both promising and physically meaningful. This effect is clearest on the 180 nm 21-parameters benchmark, where the larger search space and tighter metric coupling make selective exploration especially valuable. This has clear implications for robust and sample-efficient analog design automation.

REFERENCES

- [1] M. F. Barros, J. M. Guilherme, and N. C. Horta, *Analog circuits and systems optimization based on evolutionary computation techniques*. Springer, 2010, vol. 9.
- [2] M. Ahmadzadeh and G. G. Gielen, "Using probabilistic model rollouts to boost the sample efficiency of reinforcement learning for automated analog circuit sizing," in *Proceedings of the 61st ACM/IEEE Design Automation Conference*, 2024, pp. 1–6.
- [3] M. Ahmadzadeh, J. Lappas, N. Wehn, and G. Gielen, "Anacraft: Duel-play probabilistic-model-based reinforcement learning for sample-efficient pvt-robust analog circuit sizing optimization," *IEEE Transactions on Computer-Aided Design of Integrated Circuits and Systems*, 2025.
- [4] W. Lyu, P. Xue, F. Yang, C. Yan, Z. Hong, X. Zeng, and D. Zhou, "An efficient bayesian optimization approach for automated optimization of analog circuits," *IEEE Transactions on Circuits and Systems I: Regular Papers*, vol. 65, no. 6, pp. 1954–1967, 2017.
- [5] K. Touloupas, N. Chouridis, and P. P. Sotiriadis, "Local bayesian optimization for analog circuit sizing," in *2021 58th ACM/IEEE design automation conference (DAC)*. IEEE, 2021, pp. 1237–1242.
- [6] B. Liu, H. Zhang, X. Gao, Z. Kong, X. Tang, Y. Lin, R. Wang, and R. Huang, "Layoutcopilot: An llm-powered multi-agent collaborative framework for interactive analog layout design," *IEEE Transactions on Computer-Aided Design of Integrated Circuits and Systems*, 2025.
- [7] G. Chen, K. Zhu, S. Kim, H. Zhu, Y. Lai, B. Yu, and D. Z. Pan, "Llm-enhanced bayesian optimization for efficient analog layout constraint generation," *arXiv preprint arXiv:2406.05250*, 2024.
- [8] C. Liu, W. Chen, A. Peng, Y. Du, L. Du, and J. Yang, "Ampagent: An llm-based multi-agent system for multi-stage amplifier schematic design from literature for process and performance porting," *arXiv preprint arXiv:2409.14739*, 2024.
- [9] Y. Lai, S. Lee, G. Chen, S. Poddar, M. Hu, D. Z. Pan, and P. Luo, "Analogcoder: Analog circuit design via training-free code generation," in *Proceedings of the AAAI Conference on Artificial Intelligence*, vol. 39, no. 1, 2025, pp. 379–387.
- [10] Y. Yin, Y. Wang, B. Xu, and P. Li, "Ado-llm: Analog design bayesian optimization with in-context learning of large language models," in *Proceedings of the 43rd IEEE/ACM International Conference on Computer-Aided Design*, 2024, pp. 1–9.
- [11] N. Rouf, F. Amin, and P. D. Franzone, "Can low-rank knowledge distillation in llms be useful for microelectronic reasoning?" in *2024 IEEE LLM Aided Design Workshop (LAD)*, 2024, pp. 1–6.
- [12] Y. Wen, J. Dean, B. A. Floyd, and P. D. Franzone, "High dimensional optimization for electronic design," in *Proceedings of the 2022 ACM/IEEE Workshop on Machine Learning for CAD*, 2022, pp. 153–157.
- [13] T. Gu, J. Wang, Z. Bi, C. Yan, F. Yang, Y. Qin, T. Cui, and X. Zeng, "tss-bo: Scalable bayesian optimization for analog circuit sizing via truncated subspace sampling," in *2024 Design, Automation & Test in Europe Conference & Exhibition (DATE)*. IEEE, 2024, pp. 1–6.
- [14] D. V. Kochar, H. Wang, A. P. Chandrakasan, and X. Zhang, "Ledro: Llm-enhanced design space reduction and optimization for analog circuits," in *2025 IEEE International Conference on LLM-Aided Design (ICLAD)*. IEEE, 2025, pp. 141–148.
- [15] C. Liu and D. Chitnis, "Eesizer: Llm-based ai agent for sizing of analog and mixed signal circuit," *IEEE Transactions on Circuits and Systems I: Regular Papers*, 2025.
- [16] N. K. Somayaji and P. Li, "Llm-uso: Large language model-based universal sizing optimizer," *IEEE Transactions on Computer-Aided Design of Integrated Circuits and Systems*, 2025.
- [17] N. Shinn, F. Cassano, A. Gopinath, K. Narasimhan, and S. Yao, "Reflexion: Language agents with verbal reinforcement learning," *Advances in Neural Information Processing Systems*, vol. 36, pp. 8634–8652, 2023.
- [18] E. Nelson, G. Kollias, P. Das, S. Chaudhury, and S. Dan, "Needle in the haystack for memory based large language models," *arXiv preprint arXiv:2407.01437*, 2024.
- [19] R. S. Sutton and A. G. Barto, *Reinforcement Learning: An Introduction*, 2nd ed. Cambridge, MA: MIT Press, 2018. [Online]. Available: <https://incompleteideas.net/book/the-book-2nd.html>
- [20] R. S. Sutton, D. A. McAllester, S. P. Singh, and Y. Mansour, "Policy gradient methods for reinforcement learning with function approximation," in *Advances in Neural Information Processing Systems 12 (NeurIPS 1999)*, S. A. Solla, T. K. Leen, and K.-R. Müller, Eds. MIT Press, 2000, pp. 1057–1063.
- [21] V. Mnih, K. Kavukcuoglu, D. Silver, A. A. Rusu, J. Veness, M. G. Bellemare, A. Graves, M. Riedmiller, A. K. Fidjeland, G. Ostrovski, S. Petersen, C. Beattie, A. Sadik, I. Antonoglou, H. King, D. Kumaran, D. Wierstra, S. Legg, and D. Hassabis, "Human-level control through deep reinforcement learning," *Nature*, vol. 518, no. 7540, pp. 529–533, 2015. [Online]. Available: <https://www.nature.com/articles/nature14236>
- [22] J. Schulman, S. Levine, P. Abbeel, M. Jordan, and P. Moritz, "Trust region policy optimization," in *Proceedings of the 32nd International Conference on Machine Learning*, ser. Proceedings of Machine Learning Research, vol. 37. PMLR, 2015, pp. 1889–1897. [Online]. Available: <https://proceedings.mlr.press/v37/schulman15.html>
- [23] T. Haarnoja, A. Zhou, P. Abbeel, and S. Levine, "Soft actor-critic: Off-policy maximum entropy deep reinforcement learning with a stochastic actor," in *Proceedings of the 35th International Conference on Machine Learning*, ser. Proceedings of Machine Learning Research, vol. 80. PMLR, 2018, pp. 1861–1870. [Online]. Available: <https://proceedings.mlr.press/v80/haarnoja18b.html>
- [24] S. Fujimoto, H. van Hoof, and D. Meger, "Addressing function approximation error in actor-critic methods," in *Proceedings of the 35th International Conference on Machine Learning (ICML)*, 2018, pp. 1587–1596.
- [25] J. Schrittwieser, I. Antonoglou, T. Hubert, K. Simonyan, L. Sifre, S. Schmitt, A. Guez, E. Lockhart, D. Hassabis, T. Graepel, T. Lillicrap, and D. Silver, "Mastering atari, go, chess and shogi by planning with a learned model," *Nature*, vol. 588, no. 7839, pp. 604–609, 2020. [Online]. Available: <https://www.nature.com/articles/s41586-020-03051-4>
- [26] P. F. Christiano, J. Leike, T. B. Brown, M. Martic, S. Legg, and D. Amodei, "Deep reinforcement learning from human preferences," in *Advances in Neural Information Processing Systems 30 (NeurIPS 2017)*, I. Guyon, U. V. Luxburg, S. Bengio, H. Wallach, R. Fergus, S. Vishwanathan, and R. Garnett, Eds. Curran Associates, Inc., 2017, pp. 4299–4307. [Online]. Available: <https://papers.neurips.cc/paper/7017-deep-reinforcement-learning-from-human-preferences.pdf>
- [27] L. Ouyang, J. Wu, X. Jiang, D. Almeida, C. L. Wainwright, P. Mishkin, C. Zhang, S. Agarwal, K. Slama, A. Ray, J. Schulman, J. Hilton, F. Kelton, L. Miller, M. Simens, A. Askell, P. Welinder, P. F. Christiano, J. Leike, and R. Lowe, "Training language models to follow instructions with human feedback," in *Advances in Neural Information Processing Systems 35 (NeurIPS 2022)*, S. Koyejo, S. Mohamed, A. Agarwal, D. Belgrave, K. Cho, and A. Oh, Eds. Curran Associates, Inc., 2022, pp. 27 730–27 744. [Online]. Available: https://proceedings.neurips.cc/paper_files/paper/2022/file/b1efde53be364a73914f58805a001731-Paper-Conference.pdf
- [28] H. Wang, "Bayesian-optimization," <https://github.com/wangronin/Bayesian-Optimization>, 2023, GitHub repository.
- [29] H. Vogt, G. Atkinson, and P. Nenzi, *Ngspice User's Manual*, Sep. 2025, version 45 (ngspice release version). [Online]. Available: <https://ngspice.sourceforge.io/docs/ngspice-45-manual.pdf>
- [30] Qwen Team, "Qwen2.5-14b-instruct," <https://huggingface.co/Qwen/Qwen2.5-14B-Instruct>, 2024, model card, accessed: 2026-03-15.
- [31] A. Hurst, A. Lerer, A. P. Goucher, A. Perelman, A. Ramesh, A. Clark, A. Ostrow, A. Welihinda, A. Hayes, A. Radford *et al.*, "Gpt-4o system card," *arXiv preprint arXiv:2410.21276*, 2024.
- [32] A. Singh, A. Fry, A. Perelman, A. Tart, A. Ganesh, A. El-Kishky, A. McLaughlin, A. Low, A. Ostrow, A. Ananthram *et al.*, "Openai gpt-5 system card," *arXiv preprint arXiv:2601.03267*, 2025.
- [33] L. McInnes, J. Healy, S. Astels *et al.*, "hdbscan: Hierarchical density based clustering," *J. Open Source Softw.*, vol. 2, no. 11, p. 205, 2017.